ACS APPLIED MATERIALS & INTERFACES

Research Article

www.acsami.org

Platinum(II)-Based Metallo-Supramolecular Polymer with Controlled Unidirectional Dipoles for Tunable Rectification

Chanchal Chakraborty,[†,‡,§] Rakesh K. Pandey,[†] Md. Delwar Hossain,[†] Zdenek Futera,[‡] Satoshi Moriyama,[‡,§] and Masayoshi Higuchi*[,†,§]

[†]Electronic Functional Materials Group, National Institute for Materials Science (NIMS), Tsukuba 305-0044, Japan

[‡]International Center for Materials Nanoarchitectonics (MANA), NIMS, Tsukuba, Japan

[§]JST-CREST, Chiyoda-ku, Tokyo 102-0076, Japan

Supporting Information

ABSTRACT: A platinum(II)-based, luminescent, metallo-supramolecular polymer (PolyPtL1) having an inherent dipole moment was synthesized via complexation of Pt(II) ions with an asymmetric ligand L1, containing terpyridyl and pyridyl moieties. The synthesized ligand and polymer were well characterized by various NMR techniques, optical spectroscopy, and cyclic voltammetry studies. The morphological study by atomic force microscopy revealed the individual and assembled polymer chains of 1−4 nm height. The polymer was specifically attached on Au-electrodes to produce two types of film (films 1 and 2) in which the polymer chains were aligned with their dipoles in opposite directions. The Au-surface bounded films were characterized by UV−vis, Raman spectroscopy, cyclic voltammetry, and atomic force microscopy study. The quantum mechanical calculation determined the average dipole moment for each monomer unit in PolyPtL1 to be about 5.8 D. The precise surface derivatization permitted effective tuning of the direction dipole moment, as well as the direction of rectification of the resulting polymer-attached molecular diodes. Film 1 was more conductive in positive bias region with an average rectification ratio (RR = $I(+4\ V)/I(-4\ V)$) ≈ 20, whereas film 2 was more conducting in negative bias with an average rectification ratio (RR = $I(-4\ V)/I(+4\ V)$) ≈ 18.

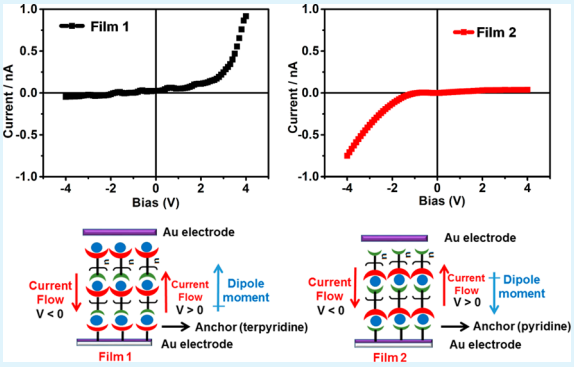

KEYWORDS: *metallo-supramolecular polymer, dipole moment, platinum(II), rectification, Au-electrode*

1. INTRODUCTION

The construction of metallo-supramolecular polymeric architectures has generated growing interest in the field of polymer and materials science providing a new dimension especially in relation to emissive materials, photovoltaics, electrochromic devices, sensors, nanowires, memory devices, nanopatterning, ionically conductive materials, catalysts, and bioconjugates.[1−5] The synthesis of nanoscale metallopolymers by a supramolecular approach and their controlled alignment between electrodes are among the most important challenges in nanochemistry, as nanoscale metallopolymers are promising materials for tunable rectifier diodes, molecular wires, and so on.[6] One possible solution to this problem might be to prepare metallo-supramolecular polymers by self-assembly of metal ions and bridging ligands, and to control the orientation of their polarity in response to an applied electric field.[7] Metallo-supramolecular polymers with a unidirectional dipole moment may be good candidates for this approach, as the orientation of their polarity can respond to an applied bias. Metallo-supramolecular polymers are usually prepared by complexation of metal ions to organic ligands possessing two similar binding sites.[8−10] Although, such polymers have no overall dipole moment. However, if the ligand itself has a net dipole moment, polymers containing the ligand will have an intrinsic net dipole aligned along the single polymer chain. This can provide an effective technique for improving the electrical properties of the polymer film.

Molecular rectifier diodes, introduced by Aviram and Ratner in 1974,[11] are highly desirable entities in molecular electronics as they have many potential applications like molecular switches, amplifiers, and sensors in advance security devices, energy harvesters, or oscillators.[12−14] Consequently, the fabrication of high-quality rectifier devices is of considerable importance in nanoscale molecular electronics. Rectification, which is produced by an asymmetric flow of electric current through a molecule under an applied potential,[15,16] results either from charge separation or a dipolar difference through a molecule.[17] In a macroscopic electrical device, a rectifier is a solid-state diode that can control the mobility of current, permitting it to flow in one direction and preventing it from

Received: April 21, 2015
Accepted: August 10, 2015
Published: August 18, 2015

ACS Publications © 2015 American Chemical Society

DOI: 10.1021/acsami.5b03434
ACS Appl. Mater. Interfaces 2015, 7, 19034−19042

flowing in the opposite direction.[18] Very recently Milko E. van der Boom group reported that the sequence-dependent assembly films of metal coordinated complexes act as molecular rectifier.[19,20] If a metallo-polymer with an inherent dipole moment is attached to an electrode by proper maintaining the orientation of its dipole moment, it is possible to tune the electronic rectification in a thin film on the electrode. In this context, we designed and synthesized a novel Pt(II)-containing, luminescent, metallo-supramolecular polymer (Scheme 1) that

Scheme 1. Synthesis of Pt(II)-Based Metallo-Supramolecular Polymer PolyPtL1

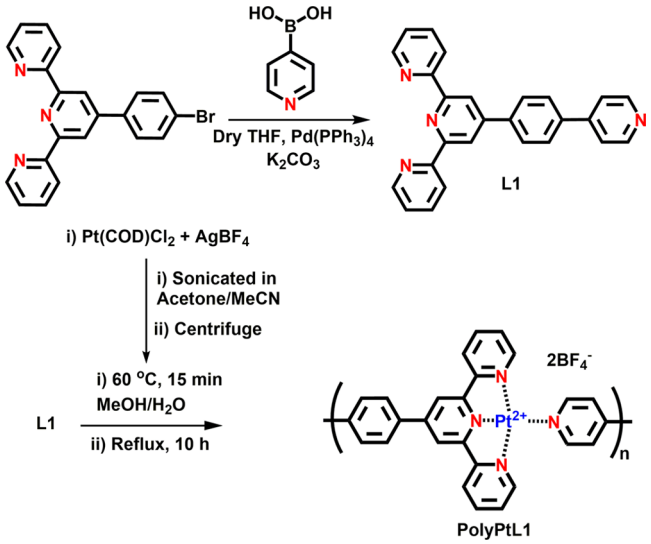

has an intrinsic dipole moment, and we attached it to Au electrodes to produce two type of films with dipole moments aligned in opposite directions, permitting reversible and complete alteration of the direction of rectification.

2. EXPERIMENTAL SECTION

2.1. Materials and Methods. Unless otherwise noted, all reagents were reagent grade and were used without purification. Dehydrated tetrahydrofuran, methanol, ethanol, dichloromethane, acetone, and acetonitrile were used as reaction solvent. The spectroscopic grade methanol was used for UV−vis and photoluminescence measurement. These solvents were purchased from Wako or Kanto Chemical Co., Inc., and used as received. Deionized water was used in the experiment where required. 4′-(4-bromophenyl)-2,2′:6′,2″-terpyridine, 4′-(4-cholorophenyl)-2,2′:6′,2″-terpyridine, 4-pyridinylboronic acid, 4-mercaptopyridine, sodium ethanethiolate, $Pt(COD)Cl_2$, $Pd(PPh_3)_4$, $AgBF_4$, and 10 nm thick Au (111) coated glass were purchased from Sigma-Aldrich Co., Ltd., and used as received.

2.2. Instrumentation. ^{1}H NMR, COSY, and ^{13}C NMR spectra were recorded at 300 and 75 MHz, respectively, on a JEOL AL 300/BZ instrument. Chemical shifts were given relative to TMS. NOESY NMR was done in JEOL-ECS-400 instrument at 400 MHz. MALDI mass spectra were measured by using AXIMA-CFR, Shimadzu/Kratos TOF Mass spectrometer. The molecular weight was measured by the viscometry-RALLS (viscometry-right angle light scattering) method in DMSO on a Viscotek 270 dual detector instrument using poly(ethylene oxide) PEO-22K as the standard (flow rate: 1 mL min^{-1}). The UV−vis spectra were recorded using a Shimadzu UV-2550 UV−visible spectrophotometer. The luminescence experiments were performed in methanol solution using a Shimadzu RF-5300PC spectrofluorophotometer. The concentrations of L1 and PolyPtL1 for the UV−vis and luminescence measurements were 120 μM in methanol with respect to each repeat unit. Wide angle XRD was done by using RINT ULTIMA III with Cu Kα radiation (λ = 1.54 Å), a generator voltage of 40 kV, and current of 40 mA. The polymer powder was placed on a glass holder and scanned in the range 2θ = 2−60° at a scan rate of 1 s/step with a step width of 0.01° at room temperature. For AFM measurements, we used Seiko Instruments, Inc. (SII), Atomic Force Microscope L-Trace (Model SPI 3800 N) in dynamic force mode (DFM), and micro cantilevers (Seiko Instruments Inc., Japan) in tapping mode with a scan rate of 0.5 Hz under air at room temperature. We used tips of type SI-DF40P2 with characteristics: T = 3.7 μm, W = 40 μm, L = 160 μm, C = 26 N/m, and f_0 = 200−400 kHz. The PolyPtL1 from methanol solution (6 μM) was drop casted on HOPG surface and air-dried prior to measurements. To complete the device fabrication a second 10 nm thick Au-strip was deposited orthogonally to first Au-electrode in polymer anchored films by sputtering Au through Sanyu Electron Quick Auto Coater SC-701AT adjusting 10 nm thickness as reported previously.[21−23] Raman spectroscopy of the compounds was done with 785 nm laser as excitation source using Raman 11 instrument (Nanophoton Corporation, Japan). Cyclic voltammetry (CV) experiment of PolyPtL1 was carried out by drop casting the methanol solution of PolyPtL1 on a glassy carbon working electrode and slowly evaporating the solution. The experiments were done in argon saturated anhydrous dichloromethane solution containing 0.1 M of tetra *n*-butyl ammonium perchlorate as supporting electrolyte in dichloromethane using an electrochemical analyzer, ALS/H CH instruments. A platinum wire was used as a counter electrode and Ag/AgCl as reference electrode. The CV was measured at different scan rates. The CV of polymer anchored Au-electrodes was carried out by taking the electrode as working electrodes and anhydrous dichloromethane solution containing 0.1 M of tetra *n*-butyl ammonium perchlorate as supporting electrolyte in dichloromethane at 100 mV/s scan rate. I−V characteristics of the films was measured by two probe method using Agilent 34401A 6−1/2 digital multimeter assembling with Standford Research System (Model SR570) low noise current preamplifier and Yokogawa 7651 programmable DC source. Short circuit may be generated from pin holes due to non-homogeneous monolayer formation over Au surface. We made 40 numbers of devices out of which 16 devices gave same results and the rest of the devices were short circuited. The percentage for the success of the measurements is ∼40%.

For the calculation of dipole moment of the PolyPtL1 polymer, we employed density functional theory in cluster boundary conditions. The long-range corrected hybrid wB97XD functional was applied. LANL08 pseudopotential and corresponding pseudobasis set were used for description of platinum atoms while Pople's 6-31G(d) all-electron basis set was considered for all other atoms.

2.3. Synthesis and Characterization of L1, L3, and PolyPtL1. *2.3.1. Synthesis of Ligand L1.* 4′-(4-Bromophenyl)-2,2′:6′,2″-terpyridine (723 mg, 1.86 mmol) and pyridine-4-boronic acid (253 mg, 2.06 mmol) were dissolved in dry THF (12 mL) in a round-bottom flask. After it was degassed, the solution was placed under N_2 atmosphere. Potassium carbonate (767.3 mg, 5.56 mmol) was dissolved in the minimum volume of water in a separate round-bottom (r. b.) flask, and degassed similarly. The catalyst $Pd(PPh_3)_4$ (90 mg, 0.08 mmol) was added to the first r. b., followed by the sodium carbonate solution. The solution was stirred at 85 °C and a further portion of pyridine-4-boronic acid (50 mg, 0.41 mmol) and $Pd(PPh_3)_4$ (20 mg, 0.017 mmol) were added after 24 h, and again stirred for another 48 h. The solvent was removed under reduced pressure and the crude residue was partitioned between dichloromethane and water. The organic layer was separated and washed with aqueous NaOH (0.1 M) (3 × 50 mL). After drying over sodium sulfate, the solvent was removed under vacuum to yield a brown solid (650 mg, 90%). Recrystallization from ethanol yielded the white crystal of the desired product.

^{1}H NMR (300 MHz, DMSO-d_6, r.t.) δ ppm: 8.78 (m, 2H), 8.76 (s, 2H), 8.68 (m, 4H), 7.99−8.08 (m, 6H), 7.80 (dd, 2H), 7.55 (q, 2H). ^{13}C NMR (75 MHz, DMSO-d_6, r.t.) δ ppm: 156.26, 155.36, 150.73, 149.75, 149.26, 146.56, 138.60, 137.64, 128.17, 128.13, 124.93, 121.58, 121.37, 118.32. MALDI-TOF: [M$^+$] calcd. for $C_{26}H_{18}N_4$: 386.153,

DOI: 10.1021/acsami.5b03434
ACS Appl. Mater. Interfaces 2015, 7, 19034−19042

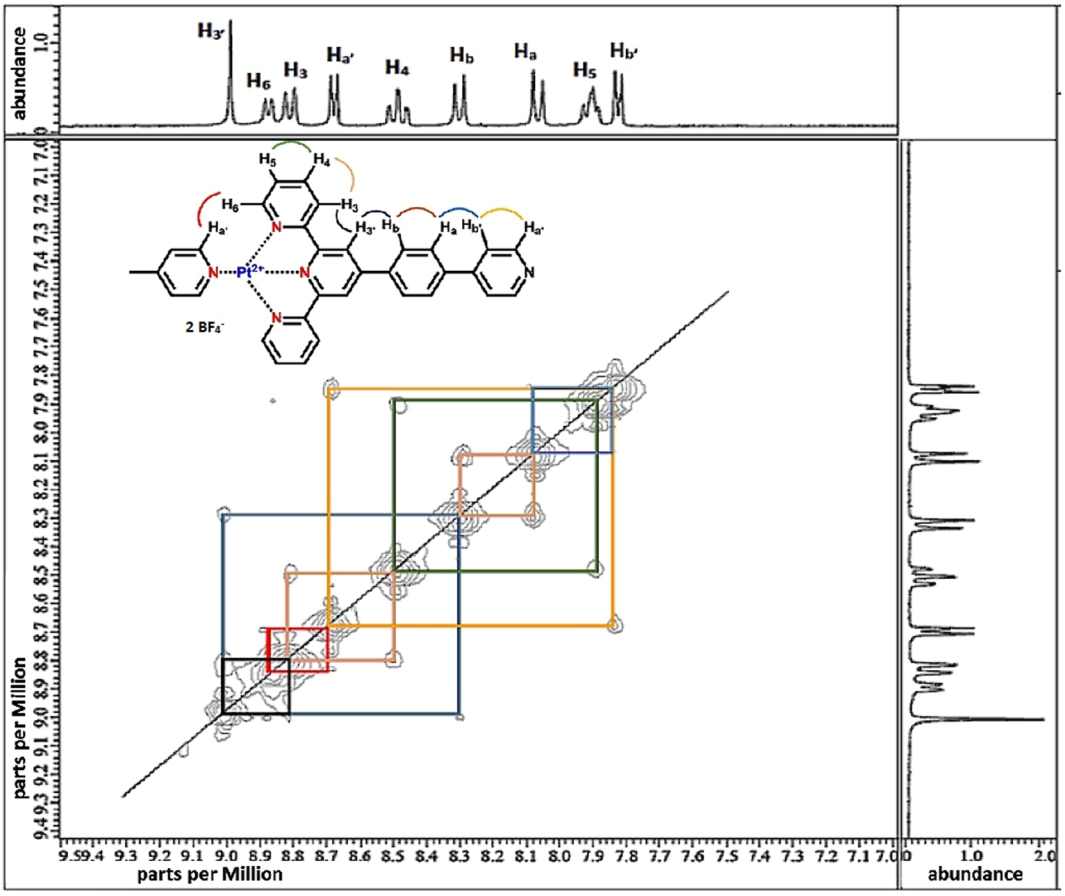

Figure 1. NOESY NMR of PolyPtL1. The red box indicated the interaction between $H_{a'}$ of pyridyl and H_6 of terpyridyl moieties.

$[(M + H)^+]$ found: 387.32. HRMS: found m/z 387.162 $[(M + H)^+]$; $C_{26}H_{18}N_4$ requires 387.161.

2.3.2. Synthesis of Ligand 4′-[4-(Mercapto)phenyl]-2,2′:6′,2″-terpyridine (L3). 4′-(4-Cholorophenyl)-2,2′:6′,2″-terpyridine (1.375 g, 4 mmol) was added with sodium ethanethiolate (1.68 g, 20 mmol) in the presence of 12 mL of anhydrous DMF under N_2. The mixture was stirred in reflux condition for 16 h and the reaction progress was monitored by TLC. The DMF was distilled off and the reaction mixture was poured into a 0.1 N HCl (60 mL). The mixture was extracted with diethyl ether and the organic layer was washed with water (50 mL × 3). The solution was dried over sodium sulfate and evaporated to dryness. Coloumn chromatography in silica gel using chloroform eluent was done with the crude product to get L3 as white solid. (1.25 g, 92%)

^{1}H NMR (300 MHz, $CDCl_3$, r.t) δ ppm: 8.73 (m, 2H), 8.69 (s, 2H), 8.67 (d, 2H, J = 8 Hz), 7.88 (td, 2H, J = 7.7 Hz, 1.8 Hz), 7.80 (dd, 2H), 7.40 (m, 2H), 7.35 (m, 2H), 3.57 (1H, s, SH) ppm. ^{13}C NMR (75 MHz, $CDCl_3$, r.t.) δ ppm: 156.32, 156.12, 149.49, 149.26, 137.02, 135.86, 132.61, 129.49, 128.01, 123.92, 121.48, 118.54 MALDI-TOF: $[M^+]$ calcd. for $C_{21}H_{15}N_3S$: 341.098, $[(M + H)^+]$ found 342.46. HRMS: found m/z 342.106 $[(M + H)^+]$; $C_{21}H_{15}N_3S$ requires 342.107.

2.3.3. Synthesis of PolyPtL1. Dichloro-1,5-cyclooctadieneplatinum-(II) (193 mg, 0.50 mmol) was treated with a solution of silver tetrafluoroborate (0.214 g, 1.1 mmol) in acetone/acetonitrile (5 mL, 4:1). The mixture was centrifuged to remove precipitated silver chloride and the supernatant solution added to a solution (methanol/water, 1:2) of ligand L1 (193.5 mg, 0.50 mmol) at 60 °C and stirred for 15 min in dark. Then the mixture was reflux at elevated temperature for overnight in dark. The yellowish brown precipitation was filtered and washed with chloroform for three times (50 mL × 3). The residue was dried to get polymer PolyPtL1 as brown solid. (320 mg, yield 84%).

^{1}H NMR (300 MHz, DMSO-d_6, r.t.) δ ppm: 9.03 (s), 8.92 (d), 8.86 (d), 8.73 (dd), 8.53 (m), 8.36 (d), 8.13 (d), 7.98 (m), 7.88 (m). Molecular weight measurement by viscometry—right-angle laser light scattering (RALLS) method; $M_w \approx 2.2 \times 10^4$ and $M_n \approx 2.0 \times 10^4$ (polydispersity index = 1.1).

3. RESULTS AND DISCUSSION

First, we synthesized the asymmetric ligand 4′-(4-pyridin-4-ylphenyl)-2,2′:6′,2″-terpyridine (L1) by Pd-catalyzed Suzuki–Miyaura cross-coupling of 4′-(4-bromophenyl)-2,2′:6′,2″-terpyridine with pyridine-4-ylboronic acid (Scheme 1). To attach the Pt ion to the terpyridyl moiety, ligand L1 was treated with a solution of a Pt(II) salt prepared by sonicating and centrifuging a mixture of $Pd(COD)Cl_2$ and $AgBF_4$ in acetone–acetonitrile (4:1) at 60 °C. On addition of the Pt salt, the color of the ligand solution changed instantaneously to yellow. Refluxing the mixture induced attachment of the pyridyl moiety to the Pt(II) ion to yield the Pt-containing metallopolymer PolyPtL1 as a yellowish brown precipitate.

Details of the characterizations of the products are provided in the Figures S1–S6. A comparison of the ^{1}H NMR spectra of PolyPtL1 and L1 in DMSO-d_6 showed a downfield shift in the proton signals of the terpyridine and pyridine moieties in the polymer (Figure S7). This significant downfield shift of the protons in PolyPtL1 is caused by attachment of Pt(II) to the terpyridyl and pyridyl moieties of L1 through complexation to form PolyPtL1. The low-intensity signals of the terminal pyridyl protons in PolyPtL1 (Figure S7) showed that the degree of polymerization (DP) was 40 and that the molecular weight (MW) of the polymer was 30 160 (this MW included

DOI: 10.1021/acsami.5b03434
ACS Appl. Mater. Interfaces 2015, 7, 19034–19042

BF_4^- counteranions). We also measured the MW by the viscometry−right-angle laser light scattering (RALLS) method; the weight-average MW (M_w) was 2.2×10^4 and the number-average MW (M_n) was 2.0×10^4 (polydispersity index = 1.1). The value of M_w was almost consistent to that estimated from the ^{1}H NMR spectrum. At lower temperature the terpyridine moieties would bind with Pt(II) to prepare PtL1 complex as terpyridine moieties have much higher reactivity with metal than pyridine moieties. At reflux condition, the pyridine moieties of L1 would bind with PtL1 to yield the PolyPtL1 polymer. So, always we assume the pyridine moieties as one terminal side and Pt at the terpyridyl end as another terminal side of the polymer chain.

For further confirmation that the metallo-supramolecular polymer PolyPtL1 was formed as desired, that is, each metal atom is attached to one terpyridyl moiety and to one pyridyl moiety, we performed a NOESY NMR and MALDI−TOF mass spectroscopic study. From the NOESY spectrum (Figure 1), we obtained insight regarding the bonded and nonbonded H interactions.

The NOESY spectrum showed a strong interaction between the Ha′ atom of the pyridyl moiety and H_6 atom of the terpyridyl moiety, which can only occur if PolyPtL1 is formed according to our proposed structure. In MALDI-TOF study, the respective masses of L1−Pt^{2+}, L1−Pt^{2+}−L1, and Pt^{2+}−L1−Pt^{2+} fragments were observed in their corresponding m/z values at 290.48, 483.20, and 194.10 respectively (Figure S8). From the study, it is confirmed that the polymer was formed as the corresponding peaks of different fragments were detected. In a wide-angle X-ray diffraction (XRD) study of PolyPtL1 (Figure S9), we observed strong signals for $\pi-\pi$ and Pt···Pt interactions[22,23] between polymer chains at d = 3.42 and 3.21 Å, respectively.

The UV−vis spectra of the ligand L1 (Figure 2) in methanol solution exhibited the structured bands between 250 and 350 nm, which were assigned to[1] ($\pi-\pi^*$) transitions associated with the coordinated terpyridyl ligand. These bands were slightly red-shifted in PolyPtL1 as a result of polymerization. The transitions a t a lower energy in PolyPtL1 (λ_{max} = 410 nm) was assigned to metal-to-ligand charge-transfer (MLCT) transitions resulting from the promotion of an electron from a Pt(d) HOMO to the LUMO π^* orbital of the terpyridyl ligand (Figure S11).[24,25] The luminescence spectra of PolyPtL1 (Figure 1) showed a strong red fluorescence at $\lambda_{max} \approx 600$ nm, assigned to Pt···Pt interactions in the 3MMLCT emissive state.[26−28] These Pt···Pt interactions have previously been identified in the wide-angle XRD studies as discussed earlier (Figure S9).

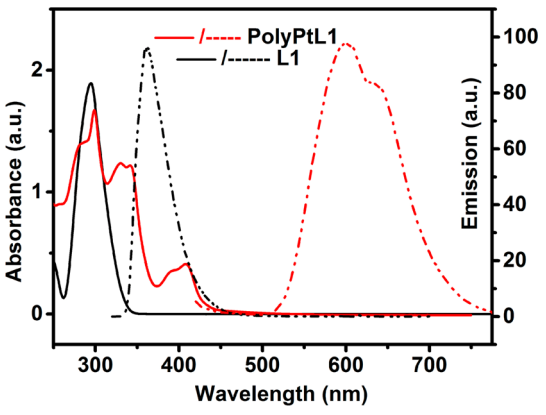

Figure 2. UV−vis and emission spectra of solutions of L1 and PolyPtL1 in methanol (120 μM with respect to repeat unit) at room temperature.

We believe the aggregation of the polymer chains is also possible in the solution state. The concentration dependent emission study of PolyPtL1 in methanol solution at room temperature was performed to explore the aggregation in solution. The study revealed that the emission intensity gradually decreased with decreasing concentration (Figure 3a). The aggregation of polymer chains can decrease with decreasing concentration which resulted the decrement of emission intensity. This study clearly showed the aggregation of polymer chains is possible there in methanol solution, too.

The solvent dependency on emission study of PolyPtL1 (Figure 3b) was also performed to evaluate the effect of solvent polarity on emission. As the solubility of PolyPtL1 was restricted only in polar solvents, we have studied the experiment using ethanol, methanol, acetonitrile and DMSO as solvent. The increasing emission intensity along with the red shifting of emission λ_{max} with decreasing solvent polarity was noticeable here. The quenching of emission with increasing solvent polarity is due to efficient LLCT radiationless decay pathway in polar solvents as the high polar solvent can significantly increase the MLCT to LLCT interconversion rate.[29,30] The red shifting of MMLCT emission of Pt(II) complexes which was previously reported in polar solvent may be due to the destabilization of the σ^* orbital and effectively lowering the energy of $d_\sigma^*-\pi^*$ (MMLCT) transition.[31]

In cyclic voltammetry study (Figure S10) of PolyPtL1 drop casted on a glassy carbon electrode from methanol solution, exhibited two reversible peaks at −1.25 and −1.8 V (vs Ag/AgCl) attributed due to the terpyridyl reduction in a Pt(II)-terpyridyl complex system.[25] A morphological study by atomic-force microscopy (AFM) (Figure 4a−d) revealed the presence of individual polymer chains and bundles of several straight polymer chains with a height of approximately 1−4 nm. The molecular dimension of a monomer unit of PolyPtL1 is derived by using Chemdraw3D software. It showed individual polymer chain height is 1.05 nm (Figure 4e). So, we can assume that the individual polymer chains can assemble to form bundles of chains by means of the strong $\pi-\pi$ and Pt···Pt interactions which were revealed earlier by XRD and emission studies.

From the structure, it is evident that L1 has an inherent dipole moment aligned from the pyridyl end to the terpyridyl end. To get further insight about the dipole moment of L1 and PolyPtL1, we employed density functional theory in cluster boundary conditions. At first, we checked the dipole moment of the L1 ligand. The dipole moment is oriented in the axial direction, as required by the symmetry of the molecule. Although, the L1 ligand is significantly asymmetric, size of the dipole moment is relatively small, 0.2 D, because of the cancellation of pyridine contributions (Figure 5a and b). Polarization of the molecule is apparent also from the highest occupied molecular orbital (HOMO), which is localized on the terpyridyl end of the molecule (Figure 5c and d). On the other hand, lowest unoccupied molecular orbital (LUMO) is placed along the main axis suggesting the conductivity of the polymer.

We considered two computational models to estimate the dipole moment of the whole PolyPtL1 polymer. In the first model, we performed calculations on the sequence of short-length oligomers (from dimer to hexamer) with uncompensated positive charges. The dipole moments of these charged

DOI: 10.1021/acsami.5b03434
ACS Appl. Mater. Interfaces 2015, 7, 19034−19042

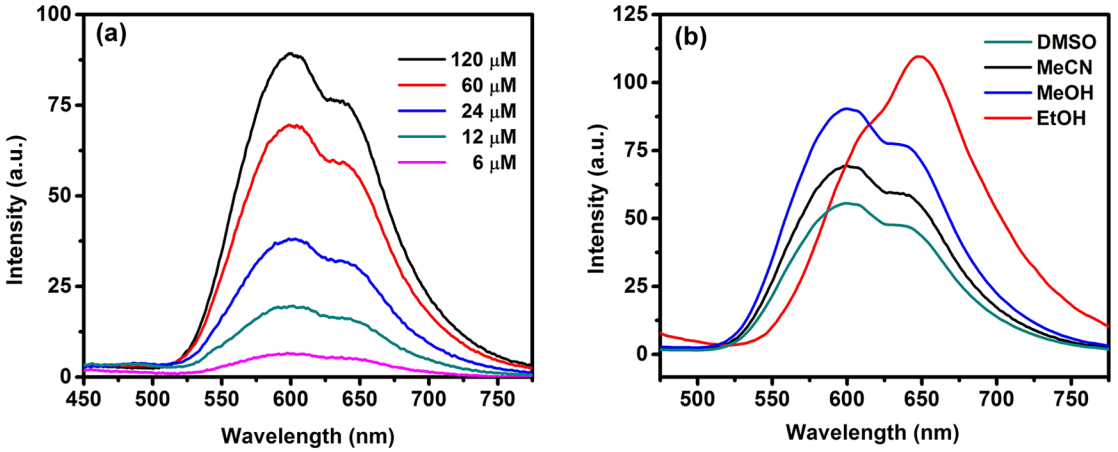

Figure 3. (a) Emission study of methanolic solution of PolyPtL1 in different concentration at room temperature. Concentration was measured with respect to each repeat unit. (b) Emission study of PolyPtL1 in different solvents.

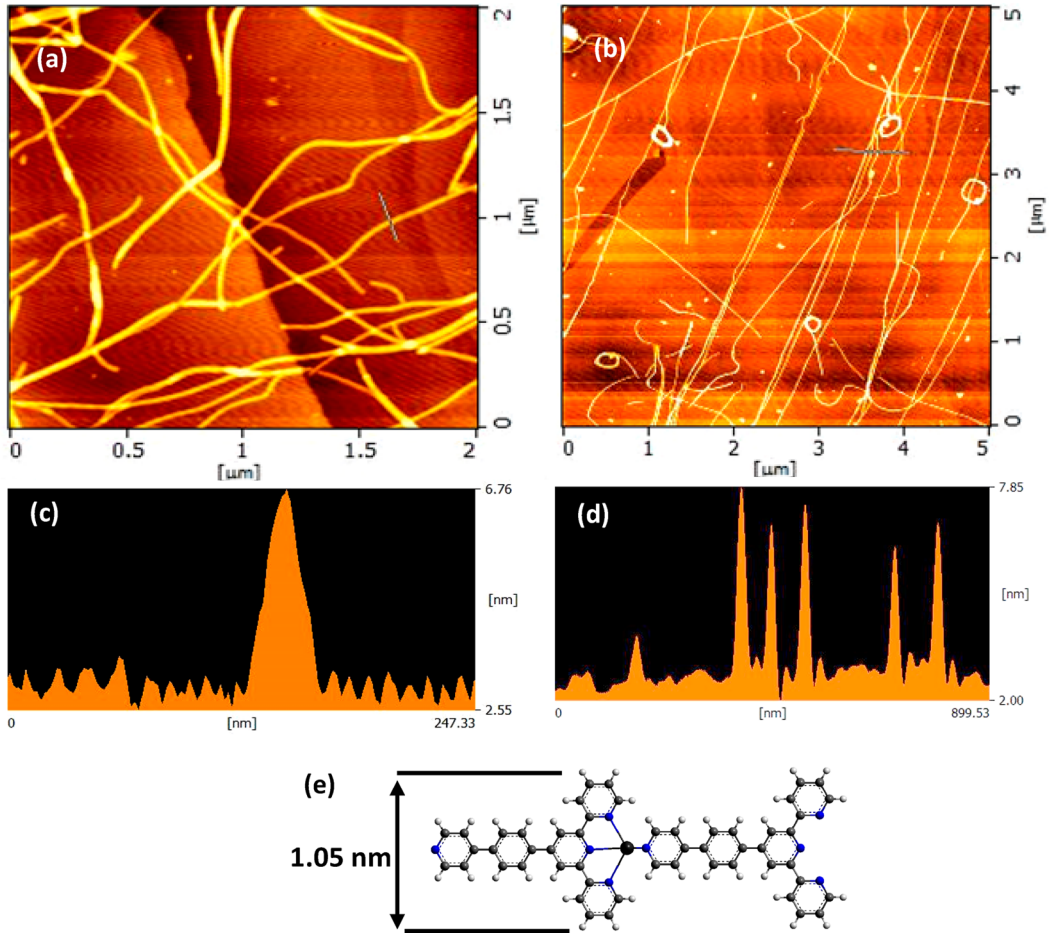

Figure 4. AFM topographic image of PolyPtL1 (a and b). Corresponding height profiles of panels a and b are shown in panels c and d. (e) Molecular dimension of a monomer unit of PolyPtL1 derived from structure in Chemdraw3D software.

structures are ill-defined (dependent on the origin of the coordinate system) and therefore, we computed atomic charges and used them to analyze polarization of the individual monomers. For comparison we calculated the atomic charges by two different approaches: (1) charge fitting to reproduce electrostatic potential (ESP) of the whole structure and (2) charges from natural population analysis (NPA) reflecting localization of the charge density on each atom. The convergence of average dipole moment of one monomer is shown in Figure 6a.

In the second model, we compensated the charge of the each Pt^{2+} cation by two BF_4^- anions that were placed to its vicinity. Positions of the anions were optimized during the structure relaxation and then the same charge analyzes were performed as in the first model. As can be seen in Figure 6b, the average dipole moment of the monomer converges to the same value as in the previous model (5.8 D in ESP approach, 4.8 D in NPA

DOI: 10.1021/acsami.5b03434
ACS Appl. Mater. Interfaces 2015, 7, 19034−19042

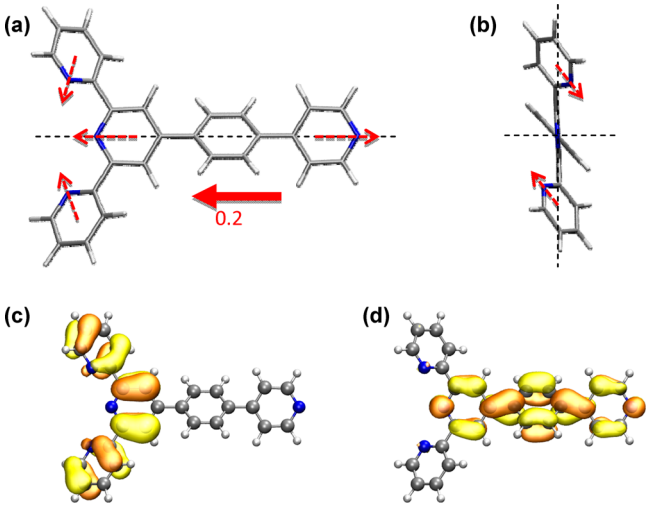

Figure 5. (a) Calculated dipole moment of the L1 (full red arrow) and its decomposition to molecular-fragment contributions (dashed red arrows). (b) Twisting of pyridine for cancellation of pyridine contributions in dipole moment. (c) Highest occupied molecular orbital (HOMO) and (d) lowest unoccupied molecular orbital (LUMO) of the L1.

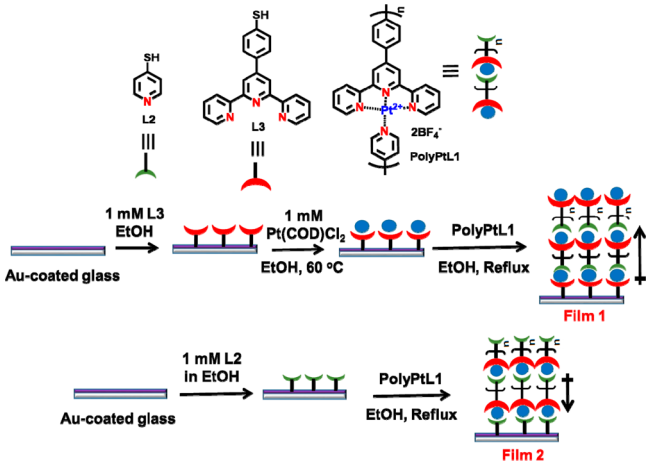

Figure 7. Preparation of films by anchoring PolyPtL1 onto a functionalized Au electrode. The directions of the dipole moments of the anchored polymer chains are shown by the arrow.

approach). The corresponding optimized structures of monomer, dimer and trimers are shown in Figure 6c-e. The enhancement in the average dipole moment of each monomer unit than L1 after complexation with Pt(II) was due to the locking of twisting of pyridine in terpyridyl moieties which can cancel out the pyridine contributions shown in Figure 5b.

To obtain insight into the molecular electronic properties of PolyPtL1, we grafted the metallo-supramolecular polymer onto functionalized Au electrodes to produce two films with their dipole moments aligned in different directions (Figure 7). The detailed procedures for anchoring the polymer to the Au electrode are discussed in Supporting Information. First, we attached a monolayer of pyridine-4-thiol (L2) or 4-(2,2′:6′,2″-terpyridin-4′-yl)benzenethiol (L3) onto the Au electrode and then we grafted PolyPtL1 to fabricate two films. In film 1, the dipole moment was oriented away from the Au electrode, whereas, in film 2, the dipole moment was oriented toward the Au electrode. To confirm the surface derivatization over Au-electrode by PolyPtL1, we examined the films by UV−vis and Raman spectroscopy and by CV. The Raman spectra shown in Figures 8a and b revealed the enhancement of Raman intensity after surface attachment of L2 and L3 on Au surface to produce their corresponding monolayers over Au.[32,33] Figure 8a showed the appearance of Au−S stretching at 316 cm^{-1} and some downfield shifting of ν_{C-S} mode from 681 to 664 cm^{-1} after attachment of L3 on Au surface.[34] Figure S13a also demonstrated that the ν_{S-H} mode of L3 at 2566 cm^{-1} was missing after monolayer formation on Au surface by L3.[33] Again, the representative peak of Pt−N stretching of PolyPtL1 at 532 cm^{-1} was also present along with other characteristic

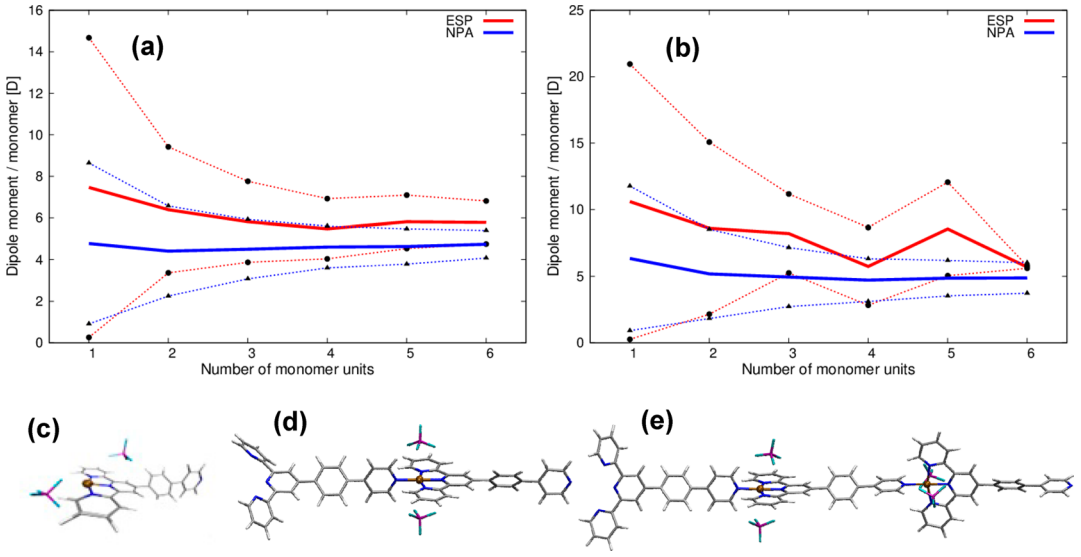

Figure 6. Convergence of the dipole moment with respect to number of monomer units x in the PolyPtL1 polymer, calculated in (a) charged model and in (b) electrostatically neutral model. Thin lines with dots represent the upper boundary (dipole moment of $L1_xPt_x$ structures with side Pt cations attached to terpyridine ending group) and lower boundary (dipole moment of $L1_xPt_{x-1}$ structures with free terpyridine ending). Thick lines show the converging averages between these two boundaries. Optimized structure of the PtL1 (c) monomer, (d) dimer, and (e) trimer. Charge of the Pt^{2+} cations are compensated by BF_4^- anions.

DOI: 10.1021/acsami.5b03434
ACS Appl. Mater. Interfaces 2015, 7, 19034−19042

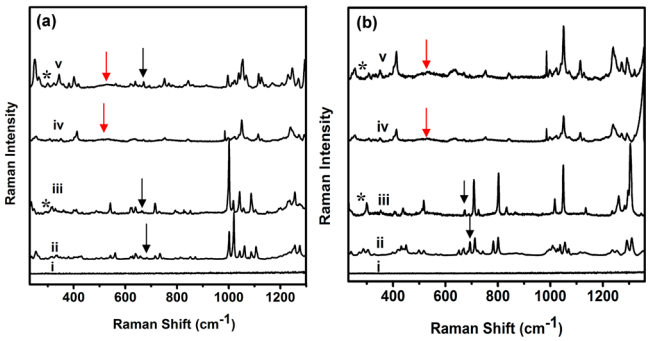

Figure 8. (a) Raman spectra of (i) Au coated glass, (ii) L3 on glass, (iii) L3 monolayer on Au-coated glass, (iv) PolyPtL1 on glass, and (v) Film 1. (b) Raman spectra of (i) Au-coated glass, (ii) L2 on glass, (iii) L2 monolayer on Au-coated glass, (iv) PolyPtL1 on glass, and (v) film 2. λ_{max} = 785 nm, 20 mW, collection time = 60 s. The stretching frequencies of Au−S, C−S, and Pt−N are shown by asterisks (*), black arrow, and red arrow, respectively.

peaks after attachment of PolyPtL1 on L3 monolayer on Au to prepare Film 1 (Figure 8a).[34] Figure 8b also exhibited the appearance of Au−S stretching at 301 cm^{-1} and some downfield shifting of ν_{CS} mode from 694 to 675 cm^{-1} after attachment of L2 on Au surface. Figure S13b also demonstrated that the ν_{SH} mode of L2 at 2570 cm^{-1} was not present after monolayer formation on Au surface by L2. Here also the representative peak of Pt−N stretching of PolyPtL1 at 532 cm^{-1} was present along with other characteristic peaks after attachment of PolyPtL1 on L2 monolayer on Au to prepare Film 2. Thus, Raman spectra of two films clearly confirmed the stepwise surface derivatization of Au surface by the polymer.

The film-state UV−vis study (Figure S14) showed a broad absorption for the ligand at about 275−375 nm and a characteristic MLCT transition of Pt(II) at ∼450 nm in both films. The appearance of MLCT transition of Pt(II) at ∼450 nm in both films confirmed the surface attachment of PolyPtL1 on Au surface. Again the cyclic voltammograms of the thin films over Au surface also (SI, Figure S15) resembled those of PolyPtL1 (SI, Figure S10). These three studies confirmed that PolyPtL1 was attached to the surface of the Au electrodes.

The attachment of thiol containing ligands and polymer over Au surface must be reflected on their surface construction. To get insight about this we performed the AFM image study of Au surface, L3 monolayer on Au and polymer attached Au surface (SI, Figure S16). From the figure, it was evident that the surface construction of Au electrode, L3 monolayer on Au and polymer attached Au surface were different. This difference in upper surface and gradually increasing height clearly confirmed the successful surface derivatization to produce Film 1.

To complete the fabrication of the device, a second 10 nm-thick Au strip was deposited orthogonally to the first Au electrode to form a sandwich of the polymer between the two Au electrodes in each film.

The electronic properties of the two films were measured by means of current−voltage (I−V) measurements. The I−V characteristics of the two films (Figure 9a and b) showed an asymmetric charge-transport behavior resulting from intrinsic polarization in the oriented sandwiched polymer chain as a result of its inherent dipole. From quantum mechanical calculations of the dipole moment and the frontier molecular orbitals (Figure 6), we determined that the average dipole moment for each monomer unit in PolyPtL1 was about 5.8 D. The nonsymmetric charge transport results of the diode films can qualitatively be explained by considering the influence of bond dipole on alignment of Fermi energy (E_F) levels of electrodes. The bond dipole can affect the surface dipole of the metal electrode and a local charge rearrangement is demonstrated induced by the anchored polymer binding a metal electrode. When the polymer chain was connected to the electrodes, the surface dipole layer induces a shift in the vacuum level (V_L) at the surface of the gold electrodes, which altered the alignment of the Fermi level (E_F) at the interface.[35,36] However, the most interesting result was that the charge-transport behavior in the two films was exactly opposite. Film 1 was more conductive under a positive bias, with an average rectification ratio RR = I(+4 V)/I(−4 V) ≈ 20, whereas Film 2 was more conducting under a negative bias, with an average rectification ratio RR = I(−4 V)/I(+4 V) ≈ 18.

The results and the observations can be explained on the basis of the model shown in Figure 10a-b. In Film 1, under a positive bias, the direction of the current flow between two electrodes was parallel to the internal dipole, as the dipole moment was oriented away from the bottom Au electrode (Figure 10a). Since, both the directions are aligned, film 1

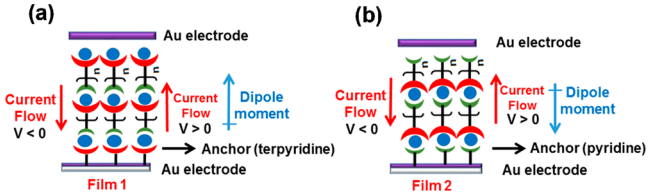

Figure 10. Crude mechanistic views of the highly conductive state of (a) film 1 at positive bias and (b) and film 2 at negative bias.

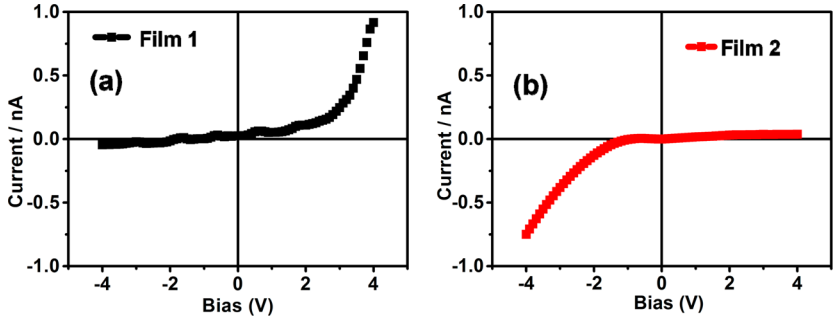

Figure 9. I−V characteristics of (a) films 1 and (b) 2 at room temperature.

DOI: 10.1021/acsami.5b03434
ACS Appl. Mater. Interfaces 2015, 7, 19034−19042

allowed to pass a high current in the positive bias region. However, under negative bias, the direction of the current flow between the two electrodes was opposite to that of the internal dipole (Figure 10a) and consequently Film 1 allowed a very low current to pass under negative bias. As film 2 has the dipole direction oriented toward the bottom Au electrode (i.e., the opposite direction to Film 1), it showed exactly opposite $I-V$ properties to those of film 1. Film 2 allowed to pass a high current only under negative bias, as the direction of the current flow between two electrodes was then parallel to the direction of the internal dipole (Figure 10b). This type of analysis has been shown mechanistically in previously reported multilayer unimolecular rectifier device systems.[14,36,37] Although, the exact position of E_F in a molecular system is very difficult to know, we can assume that the Fermi level of Au electrodes would align at the middle of the HOMO and LUMO energy gap of the molecule under a zero bias and no internal dipolar field.[36,38] For film 1, as the direction of dipole moment was away from Au electrode, it can push down the E_F of Au electrode when the device was connected with an outside circuit. This shift can lead to electron tunneling from HOMO of diode Film 1 as E_F of Au electrode was closer to the HOMO of molecular diode film.[38] On the other hand, as film 2 has opposite dipole moment direction than film 1, it can increase the E_F of Au electrode to produce an effective electron tunneling from LUMO of diode Film 2 as E_F of Au electrode was closer to the LUMO of molecular diode film. Therefore, because of the contrary dipole moment direction of two films, the opposite rectifying behavior of Film 1 and Film 2 was obtained. Again, the contacts with electrodes in both devices were different in Aul-S-Tpy-PolyPtL1 |Au and Aul-S-Py-PolyPtL1 |Au system. The contact of the top Au electrode with the SAM was a van der Waals contact, while the contact with bottom Au electrode and the SAM was covalent. So, a different potential barrier must exist due to the potential asymmetry between two contacts which can also affect the rectification.[39] However, we used same Au electrodes to overcome the problem of work function difference between electrodes. We believe that the tunability of rectification in our system is majorly by dipole moment difference between two devices as we got an approximately same rectification ratio in both devices but the only difference in direction.

4. CONCLUSION

In summary, we synthesized a new Pt(II)-based, red-luminescent, metallo-supramolecular polymer with an intrinsic dipole moment, which showed a pronounced rectifying effect when grafted onto Au electrodes. The direction of the dipole moment of the attached polymer chains on the Au electrodes could be tuned simply by changing the attachment technique. Tuning of the direction of the dipole moment affects the charge transport markedly, effectively altering the direction of rectification of the films. It should, therefore, be possible to produce polymer-based tunable rectifier diodes by using metallopolymers, which have not previously been widely used in the field of molecular electronics.

■ ASSOCIATED CONTENT

Supporting Information

The Supporting Information is available free of charge on the ACS Publications website at DOI: 10.1021/acsami.5b03434.

Characterizations of ligands and PolyPtL1 by different NMR techniques, MALDI-TOF, XRD, cyclic voltammetry, attachment of polymer on Au-electrode, its characterizations by UV−vis and Raman spectroscopy, AFM images, cyclic voltammetry, and frontier molecular orbitals HOMO and LUMO of optimized structures of Pt−L1 complex (PDF)

■ AUTHOR INFORMATION

Corresponding Author

*E-mail: HIGUCHI.Masayoshi@nims.go.jp. Tel./Fax: +81-29-860-4721.

Notes

The authors declare no competing financial interest.

■ ACKNOWLEDGMENTS

We thank to Dr. U. Rana and Dr. T. Sato for their help in various aspects of the study.

■ REFERENCES

(1) Whittell, G. R.; Hager, M. D.; Schubert, U. S.; Manners, I. Functional Soft Materials from Metallopolymers and Metallosupramolecular Polymers. *Nat. Mater.* **2011**, *10*, 176−188.

(2) Eloi, J.-C.; Chabanne, L.; Whittell, G. R.; Manners, I. Metallopolymers with Emerging Applications. *Mater. Today* **2008**, *11*, 28−36.

(3) Higuchi, M. Stimuli-responsive Metallo-supramolecular Polymer Films: Design, Synthesis and Device Fabrication. *J. Mater. Chem. C* **2014**, *2*, 9331−9341.

(4) Bandyopadhyay, A.; Sahu, S.; Higuchi, M. Tuning of Nonvolatile Bipolar Memristive Switching in Co(III) Polymer with an Extended Azo Aromatic Ligand. *J. Am. Chem. Soc.* **2011**, *133*, 1168−1171.

(5) Li, J.; Futera, Z.; Li, H.; Tateyama, Y.; Higuchi, M. Conjugation of Organic-metallic Hybrid Polymers and Calf-thymus DNA. *Phys. Chem. Chem. Phys.* **2011**, *13*, 4839−4841.

(6) Ozin, G. A.; Arsenault, A. C. *Nanochemistry*; RSC Publishing: Cambridge, U.K., 2005.

(7) Kuwahara, R.; Fujikawa, S.; Kuroiwa, K.; Kimizuka, N. Controlled Polymerization and Self-Assembly of Halogen-Bridged Diruthenium Complexes in Organic Media and Their Dielectrophoretic Alignment. *J. Am. Chem. Soc.* **2012**, *134*, 1192−1199.

(8) Kurth, D. G.; Higuchi, M. Transition Metal Ions: Weak Links for Strong Polymers. *Soft Matter* **2006**, *2*, 915−927.

(9) Burnworth, M.; Knapton, D.; Rowan, S. J.; Weder, C. Metallo-Supramolecular Polymerization: A Route to Easy-To-Process Organic/Inorganic Hybrid Materials. *J. Inorg. Organomet. Polym. Mater.* **2007**, *17* (40), 91−103.

(10) Wild, A.; Schlütter, F.; Pavlov, G. M.; Friebe, C.; Festag, G.; Winter, A.; Hager, M. D.; Cimrová, V.; Schubert, U. S. π-Conjugated Donor and Donor−Acceptor Metallo-Polymers. *Macromol. Rapid Commun.* **2010**, *31*, 868−874.

(11) Aviram, A.; Ratner, M. A. Molecular Rectifiers. *Chem. Phys. Lett.* **1974**, *29*, 277−283.

(12) Sun, L.; Diaz-Fernandez, Y. A.; Gschneidtner, T. A.; Westerlund, F.; Lara-Avila, S.; Moth-Poulsen, K. Single-molecule Electronics: From Chemical Design to Functional Devices. *Chem. Soc. Rev.* **2014**, *43*, 7378−7411.

(13) Kumar, M. J. Molecular Diodes and Applications. *Recent Pat. Nanotechnol.* **2007**, *1*, 51−57.

(14) Metzger, R. M. Electrical Rectification by a Molecule: The advent of Unimolecular Electronic Devices. *Acc. Chem. Res.* **1999**, *32*, 950−957.

(15) Wickramasinghe, L. D.; Perera, M. M.; Li, L.; Mao, G.; Zhou, Z.; Verani, C. N. Rectification in Nanoscale Devices Based on an Asymmetric Five-Coordinate Iron(III) Phenolate Complex. *Angew. Chem., Int. Ed.* **2013**, *52*, 13346−13350.

DOI: 10.1021/acsami.5b03434
ACS Appl. Mater. Interfaces 2015, 7, 19034−19042

(16) Cayre, O. J.; Chang, S. T.; Velev, O. D. Polyelectrolyte Diode: Nonlinear Current Response of a Junction between Aqueous Ionic Gels. *J. Am. Chem. Soc.* **2007**, *129*, 10801−10806.
(17) Ashwell, G. J.; Mohib, A. Improved Molecular Rectification from Self-Assembled Monolayers of a Sterically Hindered Dye. *J. Am. Chem. Soc.* **2005**, *127*, 16238−16244.
(18) Metzger, R. M. The Unimolecular Rectifier: Unimolecular Electronic Devices are Coming. *J. Mater. Chem.* **1999**, *9*, 2027−2036.
(19) de Ruiter, G.; Lahav, M.; Keisar, H.; van der Boom, M. E. Sequence-Dependent Assembly to Control Molecular Interface Properties. *Angew. Chem., Int. Ed.* **2013**, *52*, 704−709.
(20) de Ruiter, G.; Lahav, M.; van der Boom, M. E. Pyridine Coordination Chemistry for Molecular Assemblies on Surfaces. *Acc. Chem. Res.* **2014**, *47*, 3407−3416.
(21) Chen, J.; Reed, M. A.; Rawlett, A. M.; Tour, J. M. Large On-Off Ratios and Negative Differential Resistance in a Molecular Electronic Device. *Science* **1999**, *286*, 1550−1552.
(22) Pourhossein, P.; Chiechi, R. C. Directly Addressable Sub-3 nm Gold Nanogaps Fabricated by Nanoskiving Using Self-Assembled Monolayers as Templates. *ACS Nano* **2012**, *6*, 5566−5573.
(23) Ng, Z.; Loh, K. P.; Li, L.; Ho, P.; Bai, P.; Yip, J. H. K. Synthesis and Electrical Characterization of Oligo(phenylene ethynylene) Molecular Wires Coordinated to Transition Metal Complexes. *ACS Nano* **2009**, *3*, 2103−2114.
(24) Wadas, T. J.; Wang, Q.-M.; Kim, Y.-J.; Flaschenreim, C.; Blanton, T. N.; Eisenberg, R. Vapochromism and Its Structural Basis in a Luminescent Pt(II) Terpyridine−Nicotinamide Complex. *J. Am. Chem. Soc.* **2004**, *126*, 16841−16849.
(25) Yutaka, T.; Mori, I.; Kurihara, M.; Mizutani, J.; Tamai, N.; Kawai, T.; Irie, M.; Nishihara, H. Photoluminescence Switching of Azobenzene-Conjugated Pt(II) Terpyridine Complexes by Trans-Cis Photoisomerization. *Inorg. Chem.* **2002**, *41*, 7143−7150.
(26) Yam, V. W.; Chan, K. H.; Wong, K. M.; Zhu, N. Luminescent Platinum(II) Terpyridyl Complexes: Effect of Counter Ions on Solvent-induced Aggregation and Color Changes. *Chem. - Eur. J.* **2005**, *11*, 4535−4543.
(27) Bailey, J. A.; Hill, M. G.; Marsh, R. E.; Miskowski, V. M.; Schaefer, W. P.; Gray, H. B. Electronic Spectroscopy of Chloro-(terpyridine)platinum(II). *Inorg. Chem.* **1995**, *34*, 4591−4599.
(28) Grove, L. J.; Rennekamp, J. M.; Jude, H.; Connick, W. B. A New Class of Platinum(II) Vapochromic Salts. *J. Am. Chem. Soc.* **2004**, *126*, 1594−1595.
(29) Guo, F.; Sun, W.; Liu, Y.; Schanze, K. Synthesis, Photophysics, and Optical Limiting of Platinum(II) 4′-Tolylterpyridyl Arylacetylide Complexes. *Inorg. Chem.* **2005**, *44*, 4055−4065.
(30) Lu, W.; Mi, B.-X.; Chan, M. C. W.; Hui, Z.; Che, C.-M.; Zhu, N.; Lee, S.-T. Light-Emitting Tridentate Cyclometalated Platinum(II) Complexes Containing σ-Alkynyl Auxiliaries: Tuning of Photo- and Electrophosphorescence. *J. Am. Chem. Soc.* **2004**, *126*, 4958−4971.
(31) Ma, B.; Li, J.; Djurovich, P. I.; Yousufuddin, M.; Bau, R.; Thompson, M. E. Synthetic Control of Pt···Pt Separation and Photophysics of Binuclear Platinum Complexes. *J. Am. Chem. Soc.* **2005**, *127*, 28−29.
(32) Jeevagan, A. J.; John, S. A. Self-assembled Monolayer of 2,9,16,23-tetrahydroxythiophenylphthalocyanatocobalt(II) on Gold Electrode and Its Electrocatalytic Activity Towards Dioxygen Reduction. *J. Electroanal. Chem.* **2014**, *713*, 77−81.
(33) Szafranski, C. A.; Tanner, W.; Laibinis, P. E.; Garrell, R. L. Surface-Enhanced Raman Spectroscopy of Aromatic Thiols and Disulfides on Gold Electrodes. *Langmuir* **1998**, *14*, 3570−3579.
(34) Wysokiński, R.; Hernik, K.; Szostak, R.; Michalska, D. Electronic Structure and Vibrational Spectra of Cis-diammine-(orotato)platinum-(II), A Potential Cisplatin Analogue: DFT and Experimental Study. *Chem. Phys.* **2007**, *333*, 37−48.
(35) Ishii, H.; Sugiyama, K.; Ito, E.; Seki, K. Energy Level Alignment and Interfacial Electronic Structures at Organic/Metal and Organic/Organic Interfaces. *Adv. Mater.* **1999**, *11*, 605−625.
(36) Morales, G. M.; Jiang, P.; Yuan, S.; Lee, Y.; Sanchez, A.; You, W.; Yu, L. Inversion of the Rectifying Effect in Diblock Molecular Diodes by Protonation. *J. Am. Chem. Soc.* **2005**, *127*, 10456−10457.
(37) Metzger, R. M.; Chen, B.; Hopfner, U.; Lakshmikantham, M. V.; Vuillaume, D.; Kawai, T.; Wu, X.; Tachibana, H.; Hughes, T. V.; Sakurai, H.; Baldwin, J. W.; Hosch, C.; Cava, M. P.; Brehmer, L.; Ashwell, G. J. Unimolecular Electrical Rectification in Hexadecylquinolinium Tricyanoquinodimethanide. *J. Am. Chem. Soc.* **1997**, *119*, 10455−10466.
(38) Lee, Y.; Carsten, B.; Yu, L. Understanding the Anchoring Group Effect of Molecular Diodes on Rectification. *Langmuir* **2009**, *25*, 1495−1499.
(39) Nijhuis, C. A.; Reus, W. F.; Whitesides, G. M. Mechanism of Rectification in Tunneling Junctions Based on Molecules with Asymmetric Potential Drops. *J. Am. Chem. Soc.* **2010**, *132*, 18386−18401.

DOI: 10.1021/acsami.5b03434
ACS Appl. Mater. Interfaces 2015, 7, 19034−19042